Global attenuation of broadband noise fields using energy density control

Young C. Park and Scott D. Sommerfeldt
Graduate Program in Acoustics and Applied Research Laboratory, The Pennsylvania State University, P.O. Box 30, State College, Pennsylvania 16804

(Received 15 August 1995; revised 23 April 1996; accepted 7 August 1996)

The performance of the energy density control algorithm for controlling a broadband noise is evaluated in a one-dimensional enclosure. To avoid the noncausality problem of the control filter, which often happens in a frequency domain optimization, analyses presented in this paper are undertaken in the time domain. This approach provides the form of the causally constrained optimal controller. Numerical results are presented to predict the performance of the active noise control system, and indicate that improved global attenuation of the broadband noise can be achieved by minimizing the energy density, rather than the squared pressure. It is shown that minimizing the energy density at a single location yields global attenuation results that are comparable to minimizing the potential energy. Furthermore, unlike controlling the squared pressure, the energy density control does not demonstrate any dependence on the error sensor location for this one-dimensional field. A practical implementation of the energy-based control algorithm is presented. Results show that the energy density control algorithm can be implemented using the two sensor technique with a tolerable margin of performance degradation. [S0001-4966(97)02512-5]

PACS numbers: 43.50.Ki [GAD]

INTRODUCTION

Controlling the sound field in an enclosure is involved in a number of current problems of interest in active noise control. There are several active noise control algorithms derived by choosing different cost functions, such as potential energy, squared pressure, and energy density. Minimizing the potential energy yields excellent performance in terms of global attenuation.[1] However, in a practical situation, it is very difficult to measure the acoustic potential energy, so that a large number of sensors are often used to obtain an approximate measure.[2] On the other hand, the active noise control system designed to minimize the squared pressure has been widely used to control the noise in the enclosure due to the simplicity of the control structure and the efficiency in computation. However, it has been shown in previous studies[2–4] that attenuating the acoustic sound pressure at a single location in the enclosure often results in a relatively small region of control, referred to as a localized control effect.

Recently, in an attempt to simplify the control architecture, an alternative method for achieving a more global control of the sound field was developed.[3–5] This method is developed based on sensing and minimizing the energy density at discrete locations in the enclosure, so that it utilizes the concept of controlling a local variable observed at a discrete location to achieve global control. Previous work undertaken in enclosures indicates that one can often achieve improved global attenuation of deterministic signals by minimizing the acoustic energy density, rather than the squared pressure.[3–5] Also, the method has the advantage of overcoming the spillover problem that often leads to localized zones of silence when controlling the measured acoustic pressure in a field. Practical versions of such systems minimizing the energy density so far have demonstrated substantial and reliable control results in the case of deterministic signals. However, there is also a need to control broadband random noise at low frequencies in enclosures.

The objective of this study is to present numerical results that compare the global attenuation of broadband noise in a one-dimensional enclosure achieved by minimizing the energy density (which consists of the sum of the potential and kinetic energies per unit volume in the sound field), with the attenuation achieved by minimizing other acoustic parameters, such as squared pressure and potential energy. Analyses reported here are undertaken in the time domain in a manner that yields the form of the causally constrained optimal control filter.

A theoretical approach based on a frequency domain analysis enables one to establish the basic physical limitations of active noise control systems. However, this approach cannot necessarily be applied when controlling a broadband random noise, since it often yields optimal control solutions that are noncausal in the time domain,[6,7] even though such a frequency domain approach is entirely satisfactory for deterministic signals.

Another issue associated with the energy density control algorithm is that, in practical applications, multiple sensors are required to obtain error energy quantities since the acoustic velocity as well as the pressure signal should be measured to implement the algorithm.[5] In general, two microphones will be required to estimate one velocity component. Although this approach has demonstrated substantial control results, it is necessary to show that the two-microphone technique provides comparable performance to the control system employing the ideal velocity sensor. In considering a practical implementation, the optimal control filter imple-

menting the energy density control algorithm using a two-microphone sensor is presented in this paper, and its performance is demonstrated via numerical examples.

Frequency domain optimization methods based on the modal model are introduced in Sec. I. Section II presents noise control filters that are optimized under the causality constraint, and numerical results to demonstrate the performance of the optimal control filters are presented in Sec. III. Also, a two pressure microphone implementation of the energy density control is presented in Sec. IV. Section V outlines the conclusions from this work.

I. FREQUENCY DOMAIN OPTIMIZATION

The optimization of the controller in the frequency domain is based on the modal model of the sound field in an enclosure.[1,8] In this paper, the optimization is done for a one-dimensional enclosure. In addition, one primary source and one control source are considered for simplicity. To carry out this optimization, it is assumed that the enclosure is excited by a single frequency noise source. When the system is in steady state, the pressure field at the location x is given as the sum of a number of modal components,

$$p(x)=\sum_{m=0}^{\infty}(A_m+B_mQ_c)\Phi_m(x). \tag{1}$$

Here, m is the mode index, functions $\Phi_m(x)$ correspond to the eigenfunctions of the enclosure, Q_c is the complex control source strength, and the weights A_m and B_m are the modal weights associated with the primary field and the secondary control field, respectively.

The objective of the optimal control design is to compute the source strength, Q_c, so as to minimize a chosen performance function. The coefficients of the controller are optimized by using several different cost functions, such as potential energy, squared pressure, and energy density. These three performance functions can be expressed as[3]

$$I_{\mathrm{PE}}=\frac{L}{4\rho c^2}\sum_{m=0}^{\infty}|A_m+B_mQ_c|^2, \tag{2}$$

$$I_{\mathrm{SP}}=\sum_{m=0}^{\infty}\sum_{n=0}^{\infty}[A_m+B_mQ_c][A_n+B_nQ_c]^*\Phi_m(x)\Phi_n(x), \tag{3}$$

$$I_{\mathrm{ED}}=\frac{1}{2\rho c^2}\sum_{m=0}^{\infty}\sum_{n=0}^{\infty}[A_m+B_mQ_c]\times[A_n+B_nQ_c]^*F_{m,n}(x), \tag{4}$$

where

$$F_{m,n}(x)=\Phi_m(x)\Phi_n(x)+\frac{1}{k^2}\frac{\partial\Phi_m(x)}{\partial x}\frac{\partial\Phi_n(x)}{\partial x}. \tag{5}$$

Here, the subscripts PE, SP, and ED indicate cost functions corresponding to the potential energy, squared pressure, and energy density, respectively. Also, L is the length of the one-dimensional enclosure, ρ is the ambient fluid density, c is the acoustic phase speed, k is the acoustic wave number, and * denotes the complex conjugate.

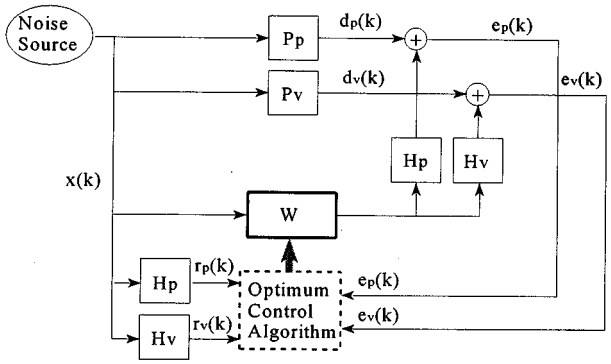

FIG. 1. A schematic diagram of the optimal noise control system.

Although the method corresponding to the potential energy is attractive for analytical work, its experimental implementation is limited by the lack of appropriate sensors to obtain a global measure of the potential energy.[2] The approach most often used in practice is the method corresponding to the cost function in Eq. (3). Since this method involves the pressure magnitude at discrete locations, it can be easily implemented. However, this approach often produces localized zones of silence instead of the desired global attenuation. The third approach, corresponding to the cost function in Eq. (4), also utilizes a local measurement, but the energy density at a discrete location yields more global information than the squared pressure control.

The results of the optimization can be expressed as[3]

$$Q_{c,\mathrm{PE}}=-\frac{\Sigma_{m=0}^{\infty}B_m^*A_m}{\Sigma_{m=0}^{\infty}B_m^*B_m}, \tag{6}$$

$$Q_{c,\mathrm{SP}}=-\frac{\Sigma_{m=0}^{\infty}A_m\Phi_m(x)}{\Sigma_{m=0}^{\infty}B_m\Phi_m(x)}, \tag{7}$$

$$Q_{c,\mathrm{ED}}=-\frac{\Sigma_{m=0}^{\infty}\Sigma_{n=0}^{\infty}A_mB_n^*F_{m,n}(x)}{\Sigma_{m=0}^{\infty}\Sigma_{n=0}^{\infty}B_mB_n^*F_{m,n}(x)}. \tag{8}$$

The method of minimizing the potential energy has been suggested as the optimal theoretical solution,[2] since it provides a global measure of the energy in the enclosure. The model and the optimization routines listed above are implemented in a simulation program, and results are presented in Sec. III.

II. TIME DOMAIN OPTIMIZATION

As a result of the frequency domain optimization over the whole frequency range, the optimal complex secondary source strengths are derived. However, the well-known disadvantage of this approach is that it often leads to highly noncausal impulse response functions in the time domain. Therefore, it is necessary to carry out the optimization in the time domain under the causality constraint to obtain optimal control filters that are causal in time.

A. Minimization of squared pressure

A digital model of the optimal noise control system is schematically illustrated in Fig. 1. A noise signal $x(k)$ is measured at the location of the noise source with a local

sensor. The same noise signal propagates both acoustically and structurally to the location of the error sensor, at which point it is desirable to remove the components due to the noise source. The controller drives the actuator to minimize certain parameters at the location of the error sensor. Hence, the error sensor measures the combined control actuator and the primary noise outputs as propagated to the error sensor location.

In Fig. 1, subscripts $_p$ and $_v$ indicate pressure and velocity parameters, respectively. The blocks P_p and P_v in Fig. 1 represent the transfer functions from the noise source to the acoustic pressure sensor and to the acoustic velocity sensor, respectively, and the blocks H_p and H_v denote the transfer functions from the adaptive filter output to the pressure and to the velocity sensors, respectively. Let $x(k), x(k-1), \ldots, x(k-N)$, and $w_0, w_1, \ldots, w_N$ represent reference input samples and tap coefficients of the Nth-order control filter implemented in a tapped-delay-line (TDL) structure, respectively. Also, let $h_{p,m}$, $0 \leqslant m \leqslant M$, denote the weights of the Mth-order finite impulse response (FIR) filter representing the impulse response from the filter output to the pressure error sensor. The sampled acoustic pressure signal detected by the pressure sensor is then equal to the sum of the primary pressure signal, $d_p(k)$, due to the primary noise source, and the control pressure signal due to the output of the actuator, so that

$$e_p(k) = d_p(k) + \sum_{n=0}^{N} w_n \sum_{m=0}^{M} h_{p,m} x(k-n-m). \tag{9}$$

Here, it was assumed that the filter weights, w_n, $0 \leqslant n \leqslant N$, are only slowly varying relative to the timescale of the response of the system to be controlled.[9] To simplify the equation, let $\mathbf{w}(k)$ and $\mathbf{r}(k)$ denote the $(N+1)\times 1$ weight vector and filtered reference input vector, respectively,

$$\begin{aligned} \mathbf{w} &= [w_0 \quad w_1 \quad \cdots \quad w_N]^T, \\ \mathbf{r}_p(k) &= [r_p(k) \quad r_p(k-1) \quad \cdots \quad r_p(k-N)]^T, \end{aligned} \tag{10}$$

where ^{T} denotes the matrix transpose, and the elements of the filtered reference input vector are defined as[8]

$$r_p(k-n) = \sum_{m=0}^{M} h_{p,m} x(k-n-m), \; 0 \leqslant n \leqslant N. \tag{11}$$

With the definitions in Eqs. (10), the pressure error signal can be rewritten as

$$e_p(k) = d_p(k) + \mathbf{w}^T \mathbf{r}_p(k). \tag{12}$$

An optimal weight vector can be obtained by minimizing the expectation of the square of the pressure error signal with respect to the weight vector $\mathbf{w}$. Thus, the optimal controller is designed by solving the following quadratic optimization problem:

$$\text{find} \quad \mathbf{w} \quad \text{minimizing} \quad J_{\mathrm{SP}} = E\{e_p^2(k)\}. \tag{13}$$

The cost function J_{SP} can be expanded out into a quadratic form:

$$J_{\mathrm{SP}} = E\{d_p^2(k)\} + 2\mathbf{w}^T \mathbf{P}_p(k) + \mathbf{w}^T \mathbf{R}_p(k) \mathbf{w}, \tag{14}$$

where $\mathbf{R}_p(k) = E\{\mathbf{r}_p(k)\mathbf{r}_p^T(k)\}$ and $\mathbf{P}_p(k) = E\{d_p(k)\mathbf{r}_p^T(k)\}$, respectively, denote the autocorrelation matrix of the filtered reference input and the cross correlation vector between the primary noise signal and the filtered reference input, associated with the acoustic pressure. Since the cost function J_{SP} has a unique minimum point, the gradient can be set to zero to obtain the optimal solution, given by

$$\mathbf{w}_{o,\mathrm{SP}} = -\mathbf{R}_p^{-1}(k) \mathbf{P}_p(k). \tag{15}$$

A signal processing problem related to the squared pressure control is to design an adaptive algorithm to minimize the square of the sensor output, and eventually obtain the optimal control signal by adjusting the weights of the control filter. A number of different control algorithms have been developed for implementing this active control approach. Those algorithms mostly rely on the filtered-x LMS algorithm[9–11] or the recursive LMS algorithm[12] due to the simplicity in implementing the algorithm.

B. Minimization of energy density

The acoustic energy density at the error sensor location in the field is expressed as

$$\xi = \frac{e_p^2(k)}{2\rho c^2} + \frac{\rho e_v^2(k)}{2}, \tag{16}$$

where $e_v(k)$ is the acoustic particle velocity signal at the same location where the pressure sensor is placed. These quantities specify the potential and kinetic energies per unit volume. Similar to the pressure error signal, the velocity error signal is also given as the sum of the primary velocity signal, $d_v(k)$, and the control velocity signal, i.e.,

$$e_v(k) = d_v(k) + \mathbf{w}^T \mathbf{r}_v(k), \tag{17}$$

where

$$\mathbf{r}_v(k) = [r_v(k) r_v(k-1) \cdots r_v(k-N)]^T \tag{18}$$

represents the filtered reference input vector associated with the acoustic velocity, whose elements are defined as

$$r_v(k-n) = \sum_{m=0}^{M} h_{v,m} x(k-n-m), \quad 0 \leqslant n \leqslant N. \tag{19}$$

Here, $h_{v,m}$, $0 \leqslant m \leqslant M$, denote the weights of the Mth-order FIR filter representing the impulse response from the filter output to the velocity error sensor. In this case, the designing of the optimal controller is accomplished by minimizing the expectation of the energy density function, given by Eq. (16), with respect to the weight vector $\mathbf{w}$. The optimization problem can be formulated as

$$\text{find} \quad \mathbf{w} \quad \text{minimizing} \quad J_{\mathrm{ED}} = \frac{E\{e_p^2(k)\}}{2\rho c^2} + \frac{\rho E\{e_v^2(k)\}}{2}. \tag{20}$$

Using Eqs. (12) and (17), the cost function J_{ED} can be expanded out into a quadratic form in the variable $\mathbf{w}$:

$$2\rho c^2 J_{\mathrm{ED}} = d_p^2(k) + (\rho c)^2 d_v^2(k) + 2\mathbf{w}^T \times [\mathbf{P}_p(k) + (\rho c)^2 \mathbf{P}_v(k)] + \mathbf{w}^T [\mathbf{R}_p(k) + (\rho c)^2 \mathbf{R}_v(k)]\mathbf{w}. \quad (21)$$

For an input noise signal that is a broadband white noise signal, this cost function is a positive definite quadratic function of the controller weights, so that it has a unique global minimum point.[5] The derivative of this cost function is expressed as

$$\nabla(2\rho c^2 J_{\mathrm{ED}}) = 2[\mathbf{P}_p(k) + (\rho c)^2 \mathbf{P}_v(k)] + 2[\mathbf{R}_p(k) + (\rho c)^2 \mathbf{R}_v(k)]\mathbf{w}. \quad (22)$$

We can set the gradient to zero to obtain the weight vector of the optimal controller:

$$\mathbf{w}_{o,\mathrm{ED}} = -[\mathbf{R}_p(k) + (\rho c)^2 \mathbf{R}_v(k)]^{-1} \times [\mathbf{P}_p(k) + (\rho c)^2 \mathbf{P}_v(k)], \quad (23)$$

where $\mathbf{R}_v(k) = E\{\mathbf{r}_v(k)\mathbf{r}_v^T(k)\}$ and $\mathbf{P}_v(k) = E\{d_v(k)\mathbf{r}_v^T(k)\}$ denote the autocorrelation matrix of the filtered reference input and the cross correlation vector between the primary noise signal and the filtered reference input, associated with the acoustic velocity, respectively. Since the energy density is controlled to try to achieve global attenuation of the sound field, the adaptive algorithm associated with the energy density-based control will involve two independent error signal components: pressure and velocity. An adaptive algorithm to obtain the optimal weight vector for the energy density control filter was fully developed and tested in Ref. 5. The algorithm in Ref. 5 was developed based on the filtered-x LMS algorithm, using an approach similar to the algorithm minimizing the sum of the squared pressure errors provided by multiple error sensors.

C. Minimization of potential energy

In a practical situation, it is very difficult to measure the acoustic potential energy, defined as the volume integral of the time-averaged acoustic potential energy density. However, to obtain an approximate measure it might be possible to use a number of acoustic pressure sensors evenly distributed over the entire enclosure. When an array of acoustic pressure sensors are used to approximate the potential energy in the one-dimensional enclosure, the cost function for the optimization can be expressed as

$$\hat{J}_{\mathrm{PE}} = \frac{1}{4\rho c^2} E\left\{ \sum_{i=0}^{N_e-1} e_p^2\left[\left(i + \frac{1}{2} \right) \delta x_e, k \right] \delta x_e \right\}, \quad (24)$$

where N_e represents total number of sensors, δx_e is distance between sensors which is equal to $1/N_e$, and $e_p[(i+\frac{1}{2})\delta x_e, k]$ is the output of the pressure error sensor located at $(i+\frac{1}{2})\delta x_e$.

The optimal control filter can be obtained by minimizing the cost function $\hat{J}_{\mathrm{PE}}$. This cost function is also a quadratic function of the controller weight vector. Furthermore, it has a unique global minimum value for the weight vector, so that the solution for $\mathbf{w}$ minimizing the potential energy in the enclosure estimated using a microphone array can be found by setting the gradient of the function $\hat{J}_{\mathrm{PE}}$ to zero. The optimal weight vector of the control filter is given by

$$\hat{\mathbf{w}}_{o,\mathrm{PE}} = -\left[\sum_{i=0}^{N_e-1} \mathbf{R}_{p,i}(k) \right]^{-1} \left[\sum_{i=0}^{N_e-1} \mathbf{P}_{p,i}(k) \right]. \quad (25)$$

Here, $\mathbf{R}_{p,i}(k)$ and $\mathbf{P}_{p,i}(k)$, respectively, represent the autocorrelation matrix and cross correlation vector corresponding to the ith sensor.

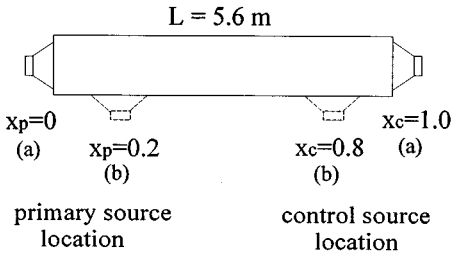

FIG. 2. System configuration considered for the computer simulation.

III. NUMERICAL RESULTS

The weight vectors of optimal controllers are derived from *ensemble averages* with the result that one filter optimum is obtained in a probabilistic sense for all realizations of the operational environment, assumed to be wide-sense stationary. However, in practical applications a nonadaptive and optimum control design involves the use of time averages, with the result that the filter depends on the number of samples used in the computation. When it is assumed that the control system is not time varying and there are sufficient input samples available, the optimal controllers are designed by minimizing time-averaged acoustic parameters, such as squared pressure, energy density, and potential energy. In this section, results from computer simulations used to test the performance of the optimal controllers are shown. In the computer simulations, the time average was used to form the cost functions being minimized.

Simulations are conducted for a one-dimensional enclosure with length $L = 5.6$ m. The simulation model considered here is presented in Fig. 2. For convenience the length of the enclosure is normalized to 1.

The model and the optimization process were implemented in simulation programs running on a PC. Based on the enclosure configuration, the frequency responses of the primary and control paths associated with the acoustic pressure and velocity were calculated using the modal model of the sound field,[1,8] with an assumed modal damping coefficient of 0.05. Impulse response estimates, i.e., p_p, p_v, h_p, and h_v, were then computed from the frequency responses. Each path was modeled as a 256-tap FIR digital filter. Prior to using the impulse response estimates in the simulation, a comparison was made between the frequency responses of the modal model and the 256-tap FIR model to establish that 256 taps was sufficient to model the primary and control paths to the accuracy required. The broadband noise signal $x(k)$ was taken to be white noise filtered through a bandpass filter with a pass band from 50 to 350 Hz, and the sampling frequency was set to 1000 Hz. Measurement noises which

are uncorrelated with the signal were added to the noise signal. The level of the measurement noise was set at -40 dB below the signal level.

Using the signal model and the impulse response estimates, 20 000 samples of the primary and the filtered reference signals were generated for both the acoustic pressure, as well as the velocity. Then, the autocorrelation matrices $\mathbf{R}_p(k)$ and $\mathbf{R}_v(k)$, and the cross correlation vectors $\mathbf{P}_p(k)$ and $\mathbf{P}_v(k)$, were estimated using the time average over the entire input samples. Finally, the weight vectors of the optimal controllers were computed using Eqs. (15), (23), and (25).

The global control of the control filter optimized in the time domain under the causality constraint was measured with the averaged power spectral density (PSD). The PSD was computed in three steps. First, frequency responses of the noise and control signal paths were calculated using the 256-tap FIR model described above. Residual signals at each of the discrete locations used were then computed using the FIR models and the noise samples. Finally, the PSD of each residual signal was computed and averaged using the equation given by

$$\overline{S(f\ )}=\frac{1}{N_o}\sum_{i=0}^{N_o-1} S\left[\left(i+\frac{1}{2}\right)\delta x_o, f\ \right], \tag{26}$$

where N_o denotes the total number of observation points, $S(x,f\ )$ is the PSD of the acoustic pressure at position x, and δx_o is the distance between adjacent observation points which is equal to $1/N_o$.

In the first configuration, denoted by (a) in Fig. 2, the primary source is positioned at one end ($x_p=0$) and the control source is placed at the other end ($x_c=1.0$). The error sensor location (x_e) is 0.7. Since the location of the error sensor is closer to the controller location than the primary source location, this configuration constitutes a causal situation for the control filter. With this configuration and FIR control filters having 64 taps, performances of the different optimization schemes were evaluated and compared with each other. Throughout the simulations, 50 microphones evenly distributed along the enclosure were used to estimate the potential energy, i.e., $N_e=50$, and the same number of microphones were used to compute the averaged PSD, i.e., $N_o=50$.

A global measure of the control that results from the frequency domain optimization is given by the potential energy in the enclosure both before and after the control is applied. In computing the optimal control strength and the potential energy, the infinite sum in Eqs. (2), (6), (7), and (8) were truncated to include the first 1500 modes. The potential energy in the enclosure as a function of frequency is shown in Fig. 3(a), and the averaged PSD achieved by using the time domain optimization is shown in Fig. 3(b), also as a function of frequency. In the figures, results obtained by minimizing the three acoustic parameters of squared pressure, energy density, and potential energy, are indicated by squared pressure control, energy density control, and potential energy control, respectively. From the results in Fig. 3(a) it can be seen that the minimization of the potential energy yields the lowest global energy, as is to be expected. However, minimizing the energy density at the single discrete location leads to results that are comparable to the results obtained by minimizing the potential energy. In fact, little difference can be found between the results indicated by energy density control and potential energy control over the entire frequency band, so that one curve is almost covered by another. On the other hand, minimizing the squared pressure actually increases the global potential energy in the enclosure at some frequencies. Furthermore, minimizing the squared pressure yields higher potential energy than minimizing the energy density as well as the potential energy at most frequencies.

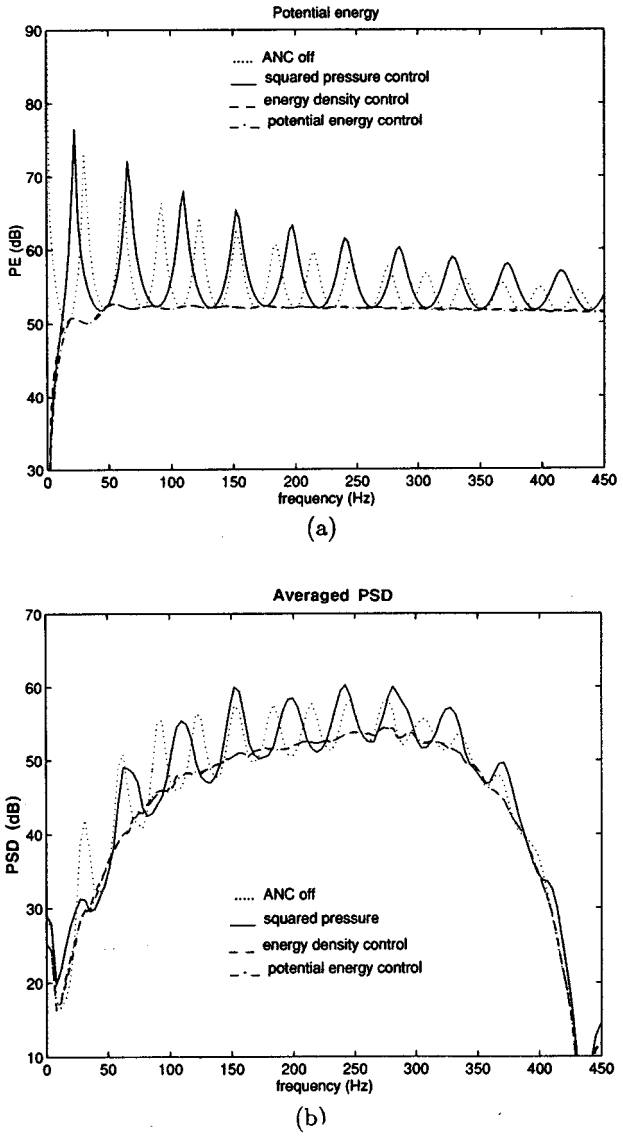

FIG. 3. Global measure of noise fields before and after the controller is applied: (a) frequency domain optimization results, (b) time domain optimization results ($x_p=0$, $x_c=1.0$, $x_e=0.7$).

Similar trends can be observed in the time domain optimization results. It should be remembered that the input signal was bandlimited from 50 to 350 Hz. Thus, the comparison between the frequency domain and time domain optimizations can be made only in that frequency range. As can be seen from Fig. 3(b), minimizing the potential energy

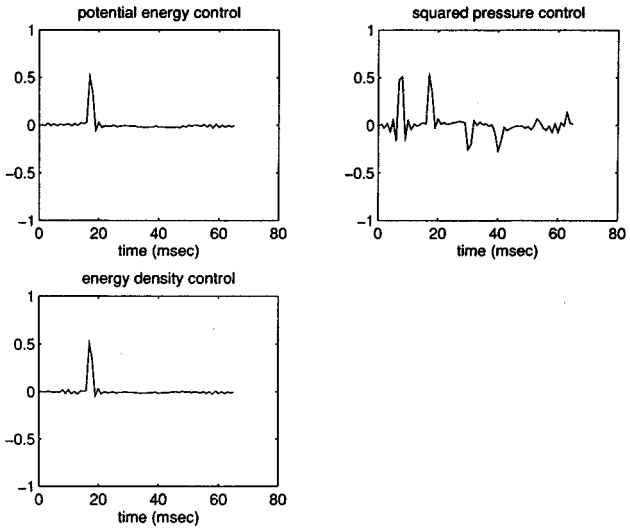

FIG. 4. Impulse responses of the optimal control filters ($x_p=0$, $x_c=1.0$, $x_e=0.7$).

yields the lowest averaged PSD results, and minimizing the energy density at a single discrete location provides results that are similar to the case of minimizing the potential energy. However, minimizing the squared pressure increases the PSD level at some frequencies, and shows poor performance at most frequencies compared to the case of minimizing the energy density as well as potential energy. Additional insight into the control effect achieved with each of the control approaches can be gained by looking at the impulse responses of the optimized controllers. Figure 4 shows the impulse responses of the FIR optimal controllers. It is clearly indicated in Fig. 4 that the energy density control provides the control filter with an impulse response which is almost identical to the one obtained by minimizing the potential energy.

In the next simulation, the error sensors were placed at the normalized position of 0.3. Since the error sensor location is closer to the primary source than the controller, this configuration would lead to a noncausal controller. Figure 5(a) shows the potential energy in the enclosure using frequency domain optimization. The averaged PSD obtained by using the time domain optimization and the corresponding impulse responses are shown in Figs. 5(b) and 6, respectively. From the results in Fig. 5(a), it can be seen that minimizing the energy density at a single discrete location leads to global potential energy results which are comparable to the case of minimizing the potential energy, while the potential energy is again significantly increased by minimizing the squared pressure at some frequencies.

However, since the configuration being tested can be considered a noncausal situation in terms of the error sensor location, the results in Fig. 5(a) cannot necessarily be used to predict the performance of the control filter being implemented in the time domain. Using the time domain optimization technique, on the other hand, one can predict the exact performance of the control filter since the optimization is undertaken in a manner that satisfies the causality constraint. Also, the control results obtained by using the time domain

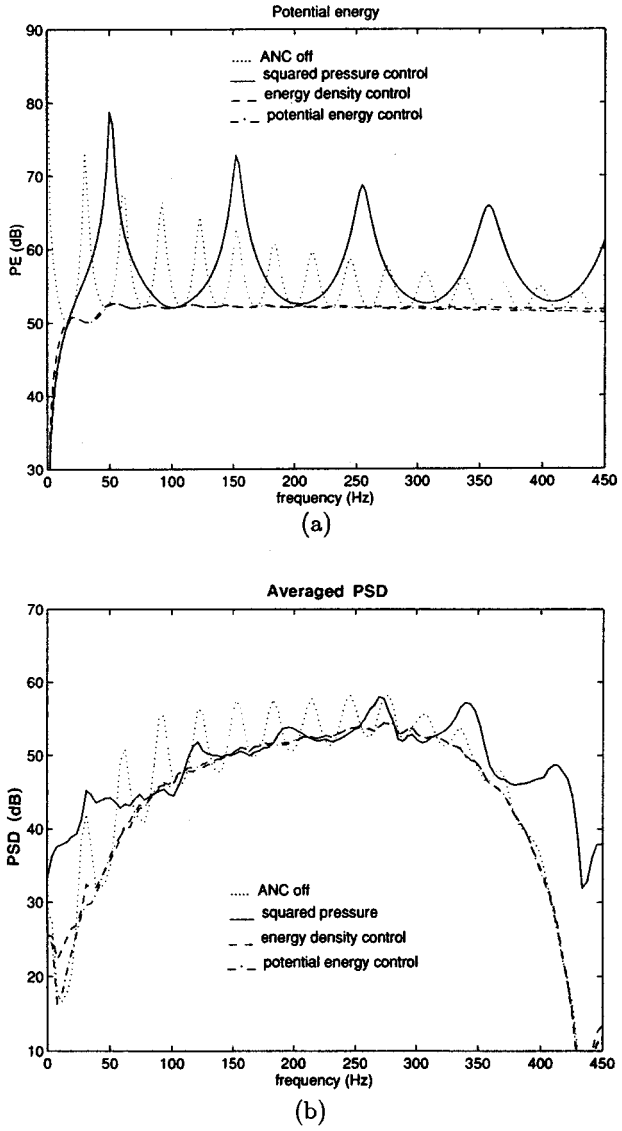

FIG. 5. Global measure of noise fields before and after the controller is applied: (a) frequency domain optimization results, (b) time domain optimization results ($x_p=0$, $x_c=1.0$, $x_e=0.3$).

optimization can differ from the results obtained by using the frequency-domain approach. As can be seen from Fig. 5, the case of minimizing the squared pressure demonstrates a difference in control results between the frequency-domain optimization and the time domain optimization. However, minimizing the squared pressure still increases the PSD levels significantly at some frequencies, the 0–100 Hz and 300–450 Hz regions in particular. However, minimizing the energy density shows the results which are similar to the case of minimizing the potential energy. Figure 6 shows the impulse responses of the optimal controllers. It is clearly shown from Fig. 6 that minimizing the energy density provides the control filter with a consistent impulse response. On the other hand, the control filter designed to minimize the squared pressure does not show the same impulse response that was obtained in the causal configuration. As a result, the algorithm yields an inconsistency in the performance as can be seen from Figs. 3(b) and 5(b). These results imply that the

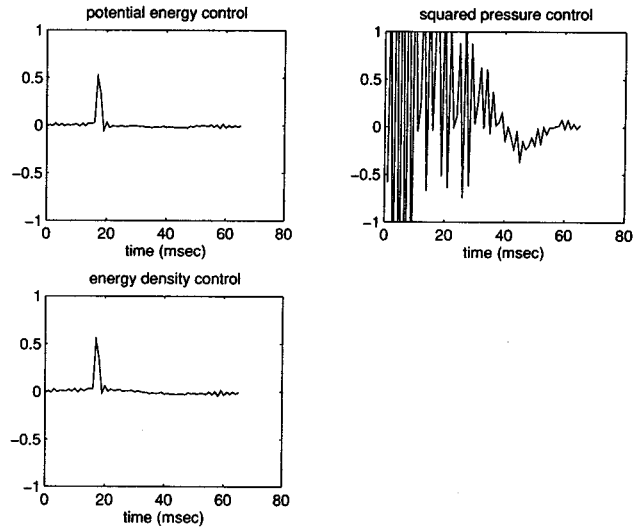

FIG. 6. Impulse responses of the optimal control filters ($x_p=0$, $x_c=1.0$, $x_e=0.3$).

performance of the controller designed to minimize the squared pressure is sensitive to the error sensor location, which imposes a limitation on practical implementations of the algorithm.

For further investigation of the inconsistency problem which may happen to the control filters in a noncausal situation, impulse responses of the optimal control filters designed to minimize the energy density and the squared pressure at several error sensor locations are illustrated in Fig. 7. The control filters were optimized for each x_e, which varies from 0.25 to 0.75. The energy density control method results in consistent control filter weights for the entire range of error sensor locations considered, while controlling the squared pressure provides highly inconsistent control filters for the error sensor locations $x_e \leqslant 0.5$, which constitute noncausal situations. The results in Fig. 7 indicate that the placement of the error sensor is not a critical issue when using energy density control, which is a significant advantage in practical applications.

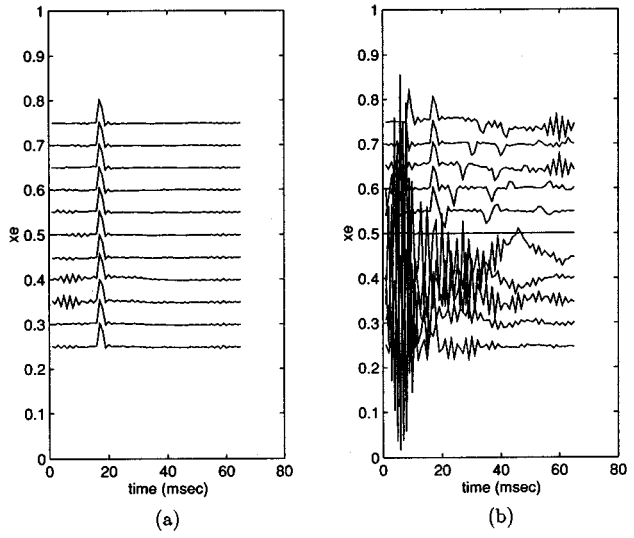

FIG. 7. Impulse responses of the control filter optimized with error sensor locations varying from 0.25 to 0.75: (a) energy density control, (b) squared pressure control ($x_p=0$, $x_c=1.0$).

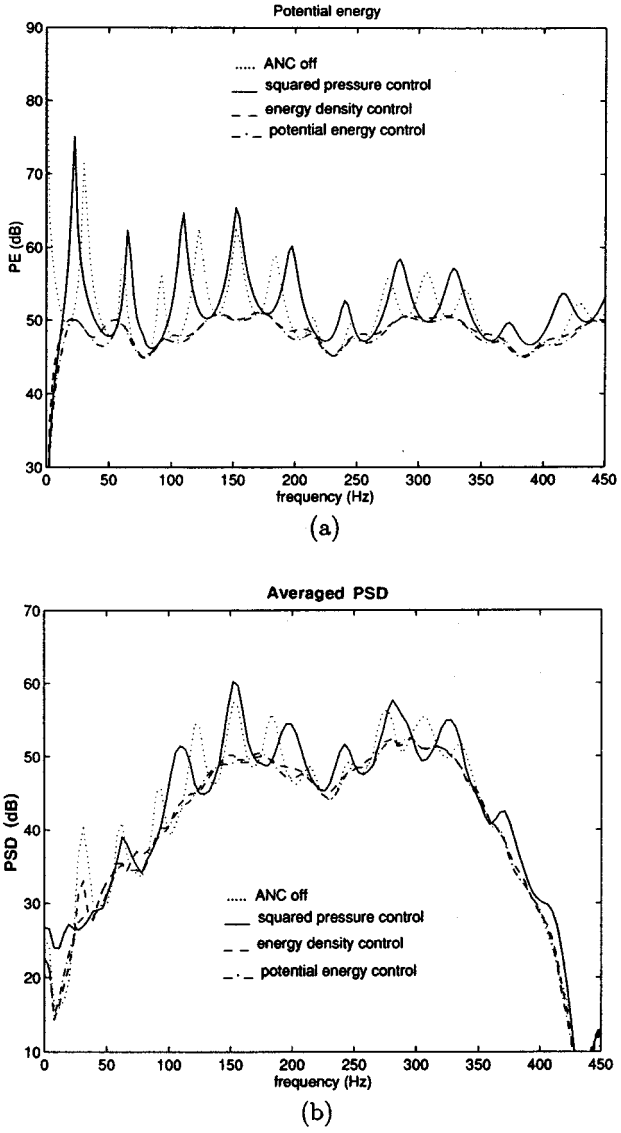

FIG. 8. Global measure of noise fields before and after the controller is applied: (a) frequency domain optimization results, (b) time domain optimization results ($x_p=0.2$, $x_c=0.8$, $x_e=0.7$).

The performance of the optimization schemes was evaluated for a different configuration of the enclosures, which is indicated by (b) in Fig. 2. In this case, the primary source is located at 0.2 and the controller is placed at 0.8. The controller position was chosen to avoid the nodal points of resonance frequencies of the enclosure, such as 30.6 Hz, 61.25 Hz, 91.8 Hz, and so on. However, it should be stated that the optimum location for the controller is not the issue investigated in this study.

Simulations were performed for two different error sensor locations: 0.7 and 0.3. Figures 8 and 9 show the results obtained with the error sensor located at 0.7. This error sensor location constitutes the configuration which provides a causal solution. Both the frequency domain optimization as well as the time domain optimization show results which are

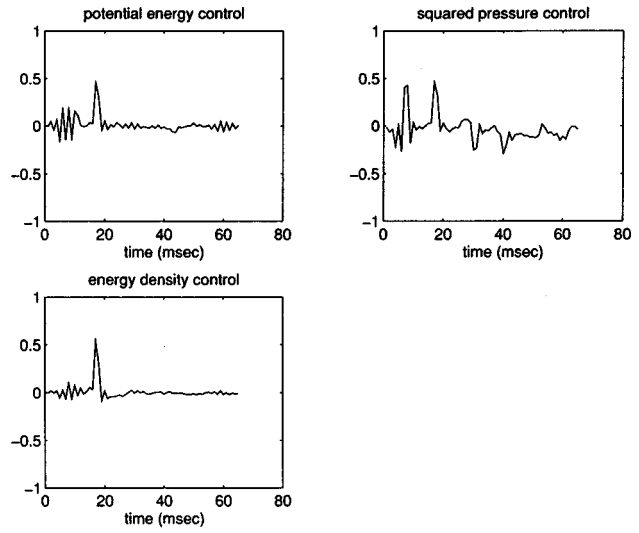

FIG. 9. Impulse responses of the optimal control filters (x_p=0.2, x_c=0.8, x_e=0.7).

similar to the previous ones obtained with the configuration x_p=0, x_c=1.0, and x_e=0.7, i.e., the energy density control shows global attenuation results which are better than the case of minimizing the squared pressure for most frequencies and comparable to the case of minimizing the potential energy.

Figures 10 and 11 show the results obtained with the error sensor located at 0.3. Minimizing the squared pressure in the time domain produces an impulse response which is different from the one obtained with the configuration x_p=0.2, x_c=0.8, and x_e=0.7. It also increases the PSD level at most frequencies. The energy density control, on the other hand, provides the control filter that is similar to the potential energy control. Figure 12 shows impulse responses of the optimal control filter designed to minimize the energy density and the squared pressure at several error sensor locations. These results again prove that, unlike the method of controlling the squared pressure, the performance of the energy density control does not depend on the error sensor location. However, the same is not true for the control source location, and, as mentioned earlier, that is not the issue of interest in this paper.

IV. IMPLEMENTATION CONSIDERATIONS FOR ENERGY DENSITY CONTROL

The implementation of the energy density control algorithm requires measurements of the acoustic velocity as well as the pressure at the error sensor location. The acoustic velocity in a one-dimensional enclosure can be obtained using a particle velocity sensor, such as a laser vibrometer or velocity microphone, or using a two-microphone technique which is typically used to measure the acoustic intensity. In this section, the energy density control algorithm is implemented in a one-dimensional enclosure, using the two-microphone technique, and its performance is evaluated.

It is generally assumed that two highly phase-matched microphones are required to obtain energy quantities when a two-microphone technique is used. However, it has been

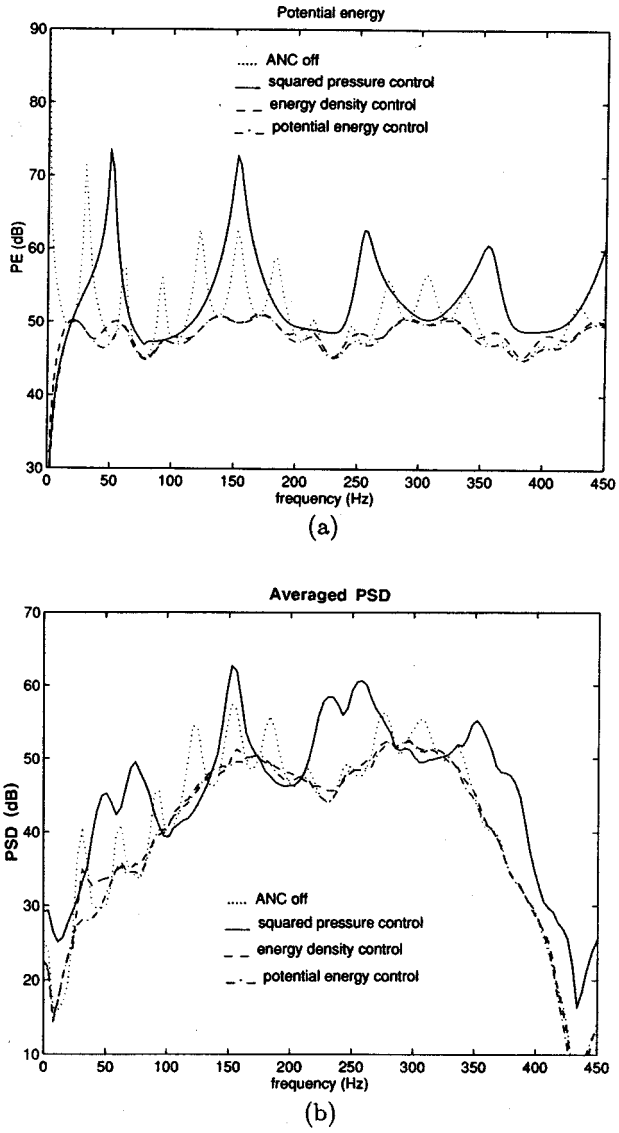

FIG. 10. Global measure of noise fields before and after the controller is applied: (a) frequency domain optimization results, (b) time domain optimization results (x_p=0.2, x_c=0.8, x_e=0.3).

shown in previous research[4,5] that low cost microphones offered by some manufacturers are sufficiently stable so that two reasonably well phase-matched microphones can be found without too much difficulty. Also, it should be mentioned that since the control system will be sensitive to all modes associated with the field in the enclosure, small measurement errors caused by the phase mismatch of the microphones are tolerable to maintain the performance desired. To conduct the analysis here, it is assumed that the magnitude and phase responses of two pressure microphones are exactly matched.

When the two sensor approach is used, the pressure and velocity in a one-dimensional enclosure are estimated using the equations, given by

$$\hat{e}_p(k)=\frac{e_{p1}(k)+e_{p2}(k)}{2}, \tag{27}$$

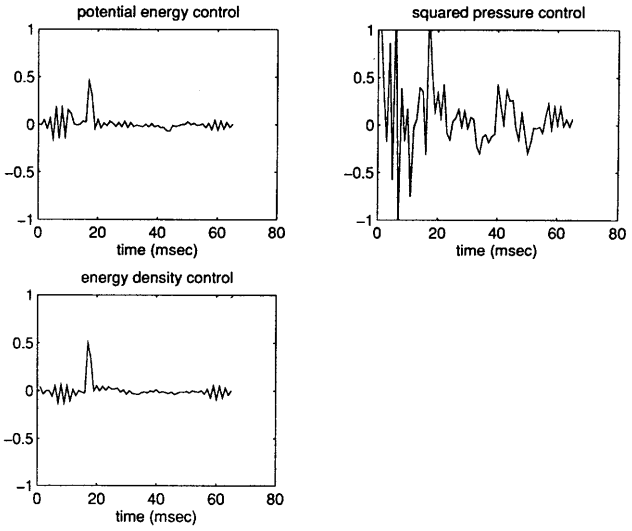

FIG. 11. Impulse responses of the optimal control filters (x_p=0.2, x_c=0.8, x_e=0.3).

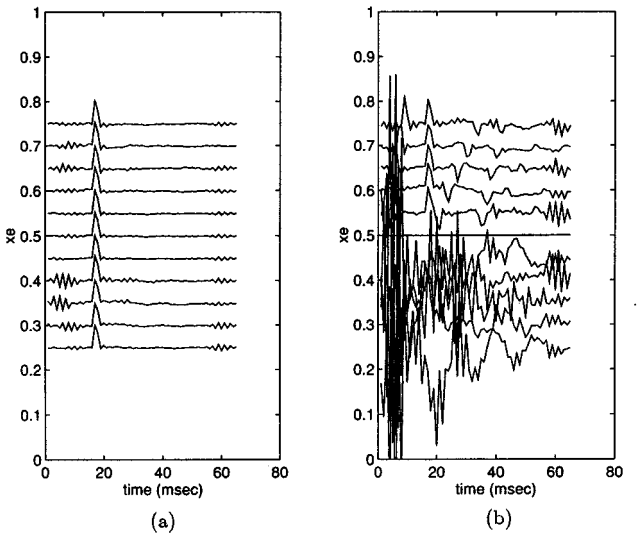

FIG. 12. Impulse responses of the control filter optimized with error sensor locations varying from 0.25 to 0.75: (a) energy density control, (b) squared pressure control (x_p=0.2, x_c=0.8).

$$\hat{e}_v(k) = -\frac{1}{\rho}\,\Xi\left\{\int_t \frac{e_{p2}(t)-e_{p1}(t)}{\Delta x}\,dt\right\}, \tag{28}$$

where $e_{p1}(k)$ and $e_{p2}(k)$ are the pressure measurements from two closely spaced microphones, Δx is the spacing between them, and $\Xi\{.\}$ denotes the continuous-to-discrete time transformation. The integration can be done using an analog integrator. However, more reliable and accurate results can be obtained by using a digital integrator. There are several possible ways of designing the digital integrators. An example of designing the digital integrator can be found in Ref. 13. Using the digital integrator, the velocity estimate can be expressed in a simple recursive form:

$$\hat{e}_v(k) = \hat{e}_v(k-1) + \alpha[e_{p2}(k)-e_{p1}(k)]\exp(-1/f_s), \tag{29}$$

where $\alpha = -1/(\rho \Delta x f_s)$ and f_s denotes the sampling frequency.

Figure 13 shows the schematic diagram of the energy density control system being implemented using the two-sensor technique. Outputs of two pressure sensors are used to estimate the acoustic pressure and velocity at the position. The estimated signals are applied to the control filter. The control filter is optimized based on the error estimates and the filtered reference inputs. To compute the filtered reference inputs, denoted by $\hat{\mathbf{r}}_p(k)$, and $\hat{\mathbf{r}}_v(k)$ in Fig. 13, the control path between the controller output and error estimates are copied to the control algorithm. In this case the control path comprises the error estimation process including the digital integrator.

Using the pressure and velocity error estimates, the weight vector of the optimal controller minimizing the energy density is expressed as

$$\hat{\mathbf{w}}_{0,\mathrm{ED}} = -[\hat{\mathbf{R}}_p(k)+(\rho c)^2\hat{\mathbf{R}}_v(k)]^{-1} \times[\hat{\mathbf{P}}_p(k)+(\rho c)^2\hat{\mathbf{P}}_v(k)], \tag{30}$$

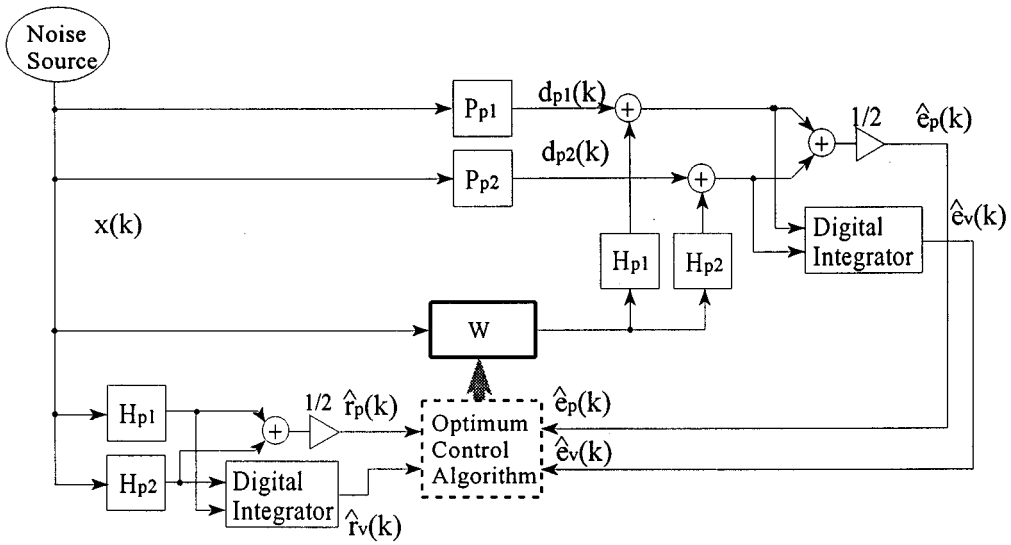

FIG. 13. Schematic diagram of the energy density control system implemented using two pressure microphones.

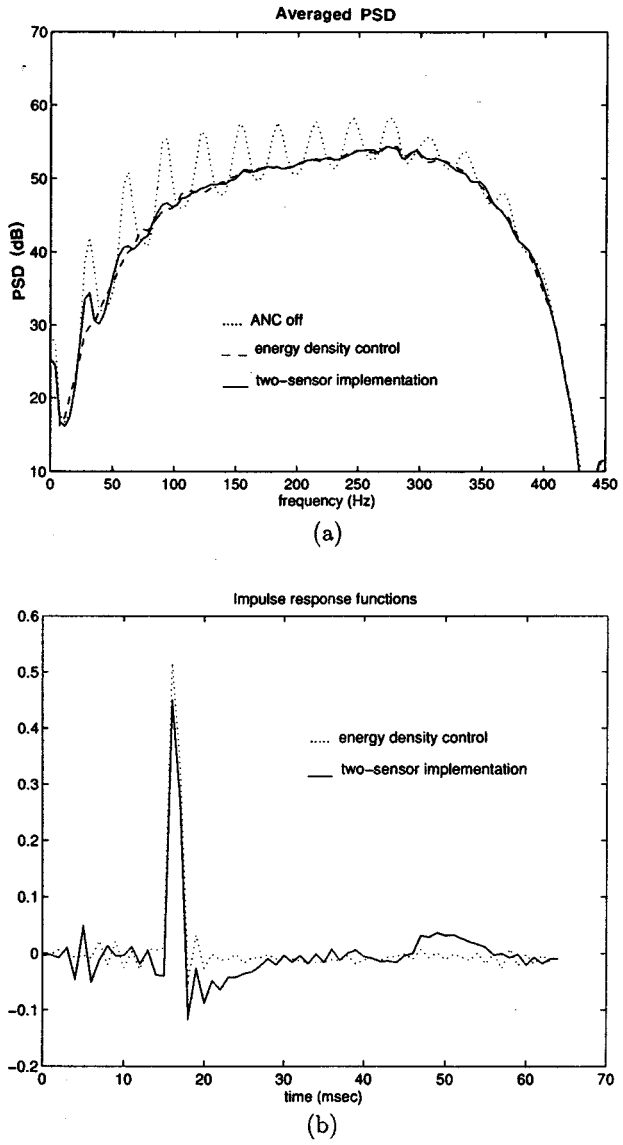

FIG. 14. The performance of the energy density control algorithm being implemented using the two-microphone technique: (a) averaged PSDs, and (b) impulse responses ($x_p=0$, $x_c=1.0$, $x_e=0.7$).

where $\hat{\mathbf{R}}_p(k)$, $\hat{\mathbf{R}}_v(k)$, $\hat{\mathbf{P}}_p(k)$, and $\hat{\mathbf{P}}_v(k)$ are the autocorrelation matrices and cross correlation matrices estimated using $\hat{\mathbf{r}}_p(k)$, $\hat{\mathbf{r}}_v(k)$.

Simulations were conducted for the case $x_p=0$, $x_c=1.0$, and $x_e=0.7$ to evaluate the performance of the two-sensor implementation. Two pressure microphones were spaced a distance of 5.0 cm (0.009 in the normalized scale). Figure 14(a) and (b) shows the averaged PSD and the impulse response. For comparison purposes, the results obtained by using the energy density control system employing the ideal velocity signal are reproduced in Fig. 14. There are several discrepancies in the results. However, overall it can be seen that the two-sensor approach yields performance which is comparable to that of the ideal energy density control. Based on these results, it can be concluded that the energy density control can be implemented using a two sensor technique without significant degradation in the performance of the original algorithm.

V. CONCLUSIONS

In this paper the performance of the energy density control method for global attenuation of broadband noise in a one-dimensional enclosure was evaluated. Numerical results were presented to compare the global attenuation achieved by minimizing the energy density with the attenuation achieved by minimizing the squared pressure or the potential energy. Optimal control filters were designed in the time domain to yield solutions that are causal in the time domain.

Numerical results have indicated that greater global control of the sound field can be achieved by minimizing the energy density, rather than the squared pressure. It has also been shown that minimizing energy density at a single location in a one-dimensional enclosure produces the global control that one would achieve by minimizing the potential energy. Another significant advantage of energy density control is that, unlike the case of minimizing the squared pressure, this control method does not demonstrate any dependence on the error sensor location. Thus, by controlling the energy density, one can overcome the limitations of the possible locations for the error sensors which exist in practical situations.

A two microphone implementation of the energy-based control algorithm was presented. Simulation results indicate that the energy density control can be implemented using the two-sensor technique with a tolerable margin of performance degradation.

[1] P. A. Nelson, A. R. D. Curtis, S. J. Elliott, and A. J. Bullmore, ''The active minimization of harmonic enclosed sound fields, Part I: Theory,'' J. Sound Vib. **117**, 1–13 (1987).

[2] A. R. D. Curtis, P. A. Nelson, and S. J. Elliott, ''Active reduction of a one-dimensional enclosed sound field: An experimental investigation of three control strategies,''J. Acoust. Soc. Am. **88,** 2265–2268 (1990).

[3] S. D. Sommerfeldt and J. W. Parkins, ''An evaluation of active noise attenuation in rectangular enclosures,'' Proc. Inter-Noise 94, Yokohama, 1351–1356 (1994).

[4] S. D. Sommerfeldt, J. W. Parkins, and Y. C. Park, ''Global active niose control in rectangular enclosures,'' Proc. Active-95, Newport Beach, CA, 477–488 (1995).

[5] S. D. Sommerfeldt and P. J. Nashif, ''An adaptive filtered-*x* algorithm for energy-based active control,''J. Acoust. Soc. Am. **96,** 300–306 (1994).

[6] A. J. Bullmore, P. A. Nelson, A. R. D. Curtis, and S. J. Elliott, ''The active minimization of harmonic enclosed sound fields, Part II: A computer simulation,'' J. Sound Vib. **117**, 15–33 (1987).

[7] S. Laugesen and S. J. Elliott, ''Multichannel active control of random noise in a small reverberant room,'' IEEE Trans. Speech Audio Process. **1**, 241–249 (1993).

[8] P. A. Nelson, and S. J. Elliott, *Active Control of Sound* (Academic, New York, 1992), Chap. 10.

[9] S. J. Elliott, I. M. Stothers, and P. A. Nelson, ''A multiple error LMS algorithm and its application to the active control of sound and vibration,'' IEEE Trans. Acoust. Speech Signal Process. **35** 1423–1434 (1987).

[10] J. C. Burgess, ''Active adaptive sound control in a duct: a computer simulation,''J. Acoust. Soc. Am. **70,** 715–726 (1981).

[11] B. Widrow and S. D. Stearns, *Adaptive Signal Processing* (Prentice-Hall, Englewood Cliffs, NJ, 1985), Chap. 11.

[12] L. J. Eriksson, M. C. Allie, and R. A. Greiner, ''The selection and application of an IIR adaptive filter for use in active sound attenuation,'' IEEE Trans. Acoust. Speech Signal Process. **ASSP-35**, 433–437 (1987).

[13] T. Hodges, P. A. Nelson, and S. J. Elliot, ''The design of a precision digital integrator for use in an active vibration control system,'' Mech. Syst. Sign. Process. **4**, 345–353 (1990).